Temperature dependence of spin-orbit torques in W/CoFeB bilayers

Witold Skowroński, Monika Cecot, Jarosław Kanak, Sławomir Ziętek, Tomasz Stobiecki, Lide Yao, Sebastiaan van Dijken, Takayuki Nozaki, Kay Yakushiji, and Shinji Yuasa

Citation: Applied Physics Letters **109**, 062407 (2016); doi: 10.1063/1.4960793
View online: http://dx.doi.org/10.1063/1.4960793
View Table of Contents: http://scitation.aip.org/content/aip/journal/apl/109/6?ver=pdfcov
Published by the AIP Publishing

Temperature dependence of spin-orbit torques in W/CoFeB bilayers

Witold Skowroński,[1,a)] Monika Cecot,[1] Jarosław Kanak,[1] Sławomir Ziętek,[1] Tomasz Stobiecki,[1] Lide Yao,[2] Sebastiaan van Dijken,[2] Takayuki Nozaki,[3] Kay Yakushiji,[3] and Shinji Yuasa[3]

[1]*AGH University of Science and Technology, Department of Electronics, Al. Mickiewicza 30, 30-059 Kraków, Poland*

[2]*NanoSpin, Department of Applied Physics, Aalto University School of Science, P.O. Box 15100, FI-00076 Aalto, Finland*

[3]*Spintronics Research Center, National Institute of Advanced Industrial Science and Technology, Tsukuba, Ibaraki 305-8568, Japan*

(Received 19 April 2016; accepted 30 July 2016; published online 12 August 2016)

We report on the temperature variation of spin-orbit torques in perpendicularly magnetized W/CoFeB bilayers. Harmonic Hall voltage measurements in perpendicularly magnetized CoFeB reveal increased longitudinal and transverse effective magnetic field components at low temperatures. The damping-like spin-orbit torque reaches an efficiency of 0.55 at 19 K. Scanning transmission electron microscopy and X-ray reflectivity measurements indicate that considerable interface mixing between W and CoFeB may be responsible for strong spin-orbit interactions. *Published by AIP Publishing*. [http://dx.doi.org/10.1063/1.4960793]

Efficient manipulation of magnetization using electrical signals at the nanoscale will further the development of next generation magnetic memories, logic,[1] and microwave devices.[2] The spin Hall effect[3] and Rashba effect[4] are intensively studied, as they produce effective magnetic fields that can be used to switch the magnetization of magnetic nano-pillars,[5] excite microwave oscillations in nano-discs,[6] or induce magnetic domain-wall motion in nanowires.[7] Quantitatively, spin-orbit torques are characterized by the spin Hall angle (θ_H), which is a measure of the ratio between spin current density (J_s) and charge current density (J_c). Different heavy metal/ferromagnet bilayers have been proposed as the source of spin-orbit torques, including Ta,[8] Hf,[9] Pt,[10] CuIr,[11] and W,[12,13] with W exhibiting the largest θ_H to date. Recent work on oxidized W has also revealed promising results.[14] Studies on the symmetry of spin-orbit torques pointed out different contributions to the effective magnetic field arising from the bulk spin Hall effect and interface Rashba interactions.[15] In addition, it has been shown that the interface between heavy metal and ferromagnetic layers strongly affects both θ_H[16] and the spin diffusion length.[17]

In this letter, we report on effective magnetic fields arising from spin-orbit interactions in W/CoFeB/MgO system. Transverse and longitudinal torques are measured in a temperature range from 19 to 300 K. Contrary to Ta buffers,[18] we find that both transverse and longitudinal torque magnitudes increase with decreasing temperature, with the longitudinal torque reaching an efficiency of 0.55 at 19 K. Considerable mixing between W and CoFeB is measured by scanning transmission electron microscopy (STEM) and X-ray reflectivity (XRR) analysis, which may be responsible for strong spin-orbit interactions in W/CoFeB bilayers.

The investigated samples consisted of sputter-deposited multilayers with the following structure: W(t_W)/$Co_{12}Fe_{68}B_{20}$ (1.3)/MgO(2.5)/Ta(4) (thicknesses in nm), with $t_W = 2$, 4, and 6 nm. After deposition, the samples were measured using vibrating sample magnetometry (VSM), X-ray diffraction (XRD), and XRR, and they were successively annealed in a high vacuum chamber. Microstructure analysis was performed using a JEOL 2200FS TEM with double Cs correctors, operated at 200 keV. Cross-sectional TEM specimens were prepared by a MultiPrep polishing machine (Allied High-Tech) and Ar ion milling. Selected samples were patterned using e-beam lithography, ion-beam etching, and lift-off processes into 70 μm long Hall bars of different width spannings from 1 to 40 μm. During microfabrication, electrical contacts with a dimension of 100×100 μm were deposited and most of the Ta top layer was etched away leaving only a thin oxidized layer as protection.

The resistivity of the samples was measured using a four-probe method, both for as-deposited devices (with in-plane magnetic anisotropy) and annealed ones (with effective perpendicular magnetic anisotropy - PMA). The harmonic Hall voltage measurements were carried out using lock-in amplification in a Janis cryogenic probe station equipped with an electromagnet. During these experiments, the temperature was varied between 19 and 300 K. Measurements were performed for various magnetic field orientations: perpendicular to the sample plane (along z axis - i.e., anomalous Hall effect (AHE) configuration), longitudinal to the stripe (along x axis), and transverse to the stripe (along y axis).

First, the crystallographic phases of W with different layer thicknesses ($t_W = 2$, 4, and 6 nm) were determined using XRD measurements. The θ–2θ scans of Fig. 1(a) reveal that the β-tungsten phase is present in all samples, whereas a clear α-tungsten reflection is visible only for the sample with a 6 nm thick W layer. The same conclusion can be drawn from four-point resistivity measurements. Assuming a CoFeB resistivity of 113 $\mu\Omega$ cm (measured independently) and a parallel resistor model, the calculated W resistivity (ρ_W) amounts to 128 and 105 $\mu\Omega$ cm for $t_W = 2$ nm and 4 nm, respectively, but it decreases significantly to 36 $\mu\Omega$ cm for $t_W = 6$ nm,

a)Electronic mail: skowron@agh.edu.pl

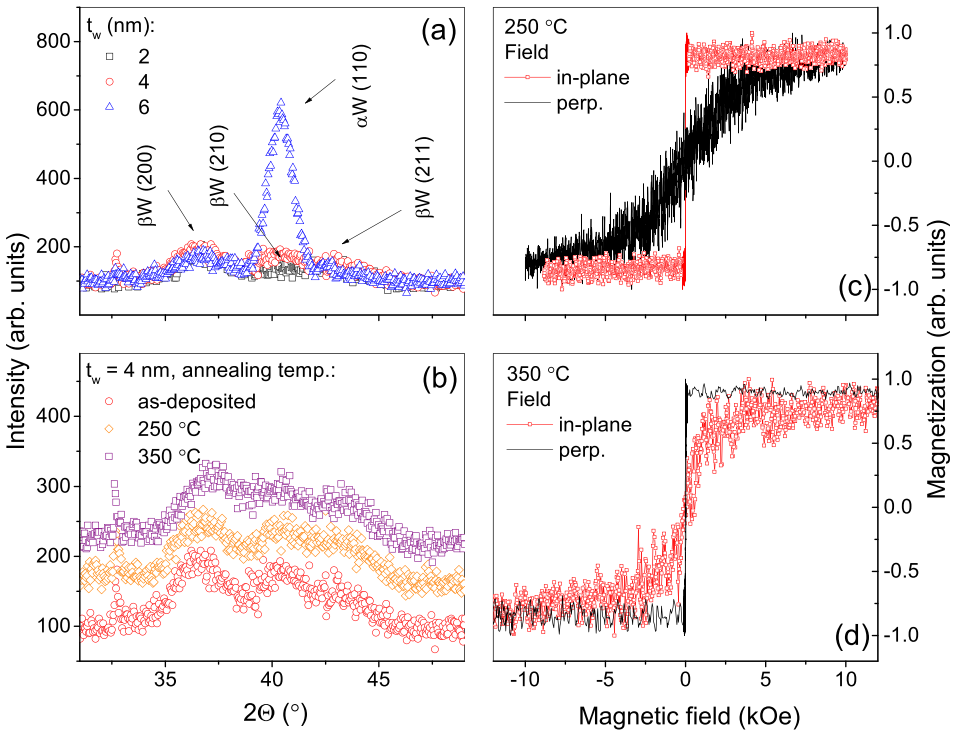

FIG. 1. XRD θ-2θ scans for as-deposited samples with different t_W (a) and for annealed samples with $t_W = 4$ nm (b) - curves are offset for clarity. In-plane and perpendicular magnetization curves for the sample with $t_W = 4$ nm after annealing at 250 °C (c) and 350 °C (d).

supporting the presence of a low-resistive α-tungsten phase.[19] We also verified that α-tungsten does not form in the thinner W layers during annealing (Fig. 1(b)). Because the β-tungsten phase is crucial for obtaining PMA and large spin Hall angles,[20] we focus on the thinner W buffers only. We note that the resistivity of W/CoFeB bilayers did not change (within experimental error) upon annealing.

Independently, the magnetic properties of the deposited stacks were verified using VSM. Exemplary magnetic hysteresis loops for $t_W = 4$ nm are presented in Fig. 1. The measurements indicate a transition from in-plane anisotropy to PMA after annealing at 350 °C, which is consistent with our earlier work.[21]

Next, the AHE of samples with $t_W = 2$ and 4 nm were measured in perpendicular magnetic field (Fig. 2). Although both W layers induce PMA in CoFeB, the switching for $t_W = 2$ nm is more abrupt compared to $t_W = 4$ nm. This effect, which can be attributed to more gradual magnetization rotation or magnetic domain formation,[22] hampers the extraction of effective magnetic fields. We note that this behavior persists even at low temperatures (inset in Fig. 2), ruling out superparamagnetism in 1.3 nm thick CoFeB as its origin. Because of the dependence of PMA on buffer thickness, we limit our discussion to effective magnetic fields in W/CoFeB bilayers with $t_W = 2$ nm. For thicker buffers, the PMA was too weak to reliably measure the effective fields.

Figure 3 shows AHE and harmonic Hall voltages at T = 19 K for the sample with $t_W = 2$ nm. The first harmonic Hall voltage signal measured in a magnetic field applied longitudinal to the Hall bar (H_L) exhibits a parabolic shape and it was fitted using a quadratic function for the magnetization pointing along $+z$ and $-z$ directions. Results for a magnetic field applied transverse to the long axis of the Hall bar (H_T) are almost identical (not shown). Likewise, the second harmonic signal was fitted using a linear function for both perpendicular magnetization directions. In this case, the two fitted lines are either symmetric (measurement along H_L - Fig. 3(c)) or asymmetric (measurement along H_T - Fig. 3(d)) with respect to the polarity of magnetic field. The model presented in Ref. 23 was used to calculate the effective longitudinal ΔH_L and transverse ΔH_T magnetic fields

$$\Delta H_{L(T)} = -2\frac{B_{L(T)} \pm 2rB_{T(L)}}{1-4r^2}$$
$$B_{L(T)} = -2\frac{\partial V^{2\omega}}{\partial H_{L(T)}} \Big/ \frac{\partial^2 V^{1\omega}}{\partial H_{L(T)}^2}, \quad (1)$$

where r is the ratio of planar Hall resistance (PHR) to anomalous Hall resistance (AHR) and the $\pm$ sign corresponds to the perpendicular magnetization direction. We measured a

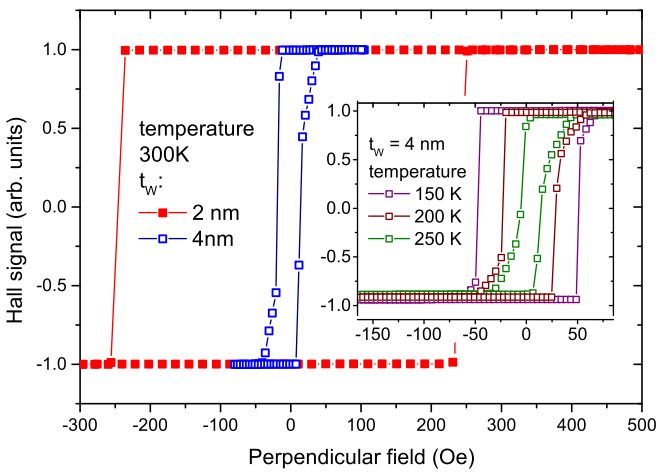

FIG. 2. AHE vs. perpendicular magnetic field measured at room temperature for samples with $t_W = 2$ (full symbols) and 4 nm (open symbols). The inset presents the AHE signal for $t_W = 4$ nm measured at various temperatures.

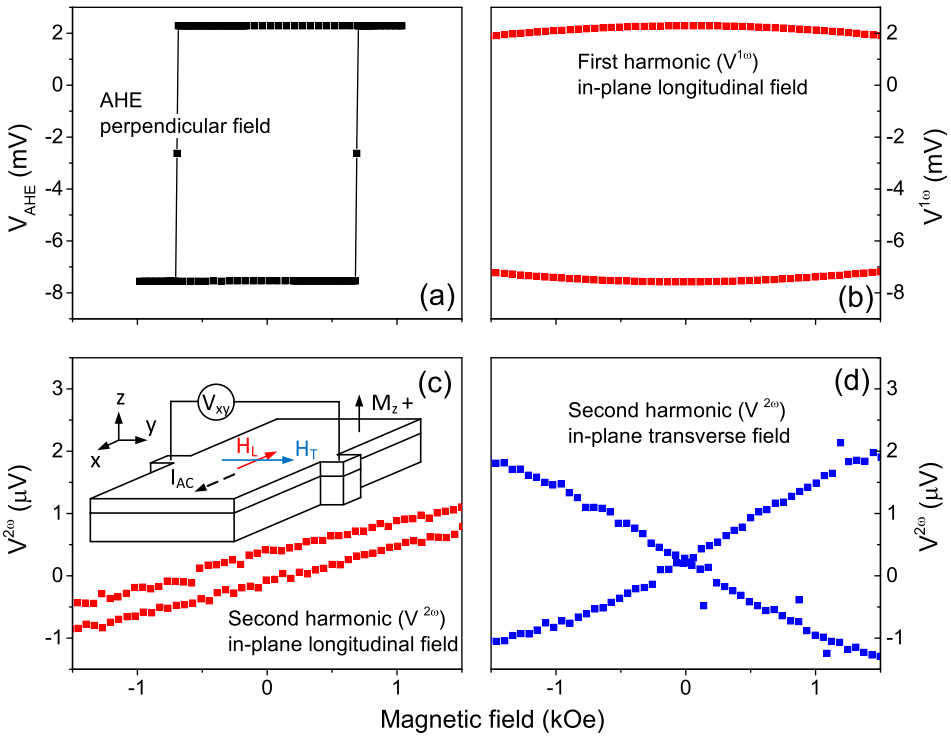

FIG. 3. (a) AHE vs. perpendicular magnetic field, (b) first harmonic Hall voltage vs. longitudinal in-plane field, (c) and (d) second harmonic Hall voltage vs. longitudinal and transverse field, respectively, obtained at T = 19 K for $t_W = 2$ nm. Note that the first Harmonic Hall voltage signal vs. transverse field is similar to (b). The inset in (c) shows the harmonic Hall voltage measurement configuration.

relatively large PHR/AHR ratio of $r = 0.3$,[24] which was included in our analysis of spin-orbit torques.

Using a parallel resistor model, we calculated the current density in the W buffer layer as $J_c = 2.17 \times 10^{10}$ A/m^2. J_c drops by about 3% at T = 19 K with respect to the room temperature value, as the resistance increases with decreasing temperature. This negative temperature coefficient is explained by the existence of an amorphous phase in the W buffer and will be discussed in detailed elsewhere. The data presented here were measured in a 10-μm-wide stripe; however, no significant dependence of the strip's width on the determined values of effective magnetic field was found. Instead of θ_H, we characterized our bilayers using damping-like and field-like spin-orbit torque efficiencies (ξ_L and ξ_L, respectively), as we independently measured these two torque components. The following equation was used to calculate the effective spin-orbit torques:

$$\Delta H_{L(T)}/J_e^W = \hbar \xi_{L(T)}/2eM_s t'_{CoFeB}, \qquad (2)$$

where $\hbar$ is the reduced Planck's constant, e is the electron charge, M_s is the saturation magnetization, and t'_{CoFeB} is the effective thickness of CoFeB: $t'_{CoFeB} = 0.92$ nm (comparing to $t_{CoFeB} = 1.3$ nm nominal thickness, without a magnetic dead layer taken into account).[21] The saturation magnetization of CoFeB at room temperature equals $\mu_0 M_s = 1.6$ T and it increases to 2 T at T = 19 K. Figure 4 presents the effective magnetic fields and spin-orbit torque efficiencies vs. temperature.

The result for ξ_L determined at room temperature is in good agreement with spin Hall angles for W buffer layers in literature.[12,13,20] A slightly higher value is expected for thicker W, as $t_W = 2$ nm used here is smaller than the spin diffusion length of W.[20] The temperature dependence of the longitudinal spin-orbit-torque is similar to Ta.[18] On the other hand, the magnitude of the transverse effective field decreases with increasing temperature, which is qualitatively different compared to Ta buffers. In order to explain this discrepancy and to shed some light on the large spin Hall angles that are reported in W/CoFeB bilayers, we studied the interface between these two layers using STEM and XRR analysis.

Figure 5 presents a Z-contrast STEM image. The chemical sensitivity of the high-angle scattered electron signal provides good contrast between the polycrystalline W buffer, CoFeB/MgO bilayer, and the Ta film with a thin oxidized layer on top. The line scan in Fig. 5(b) shows a gradual change of Z-contrast near the W/CoFeB interface, providing proof of considerable intermixing between these two layers. This observation is further corroborated by the XRR

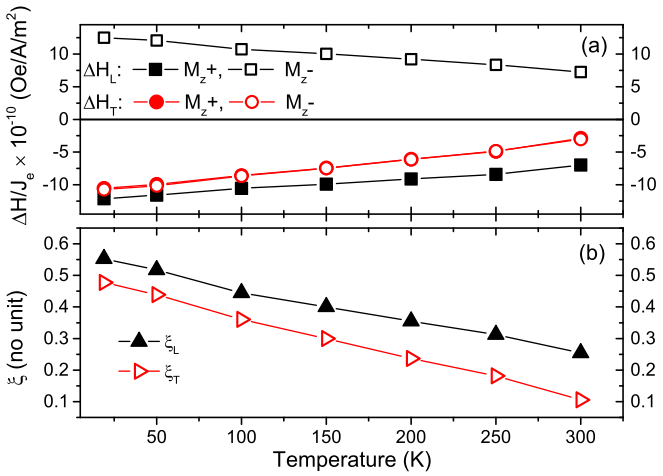

FIG. 4. (a) $\Delta H_L/J_e$ and $\Delta H_T/J_e$ as a function of temperature measured for a 10-μm-wide stripe with $t_W = 2$ nm. The Oersted field contribution was calculated from the current flowing through the buffer and subtracted from the transverse field. (b) Spin Hall efficiency as determined from Eq. (2).

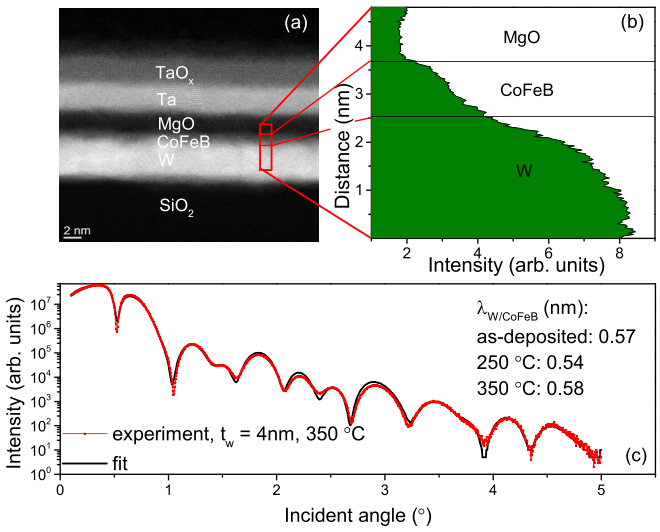

FIG. 5. Z-contrast STEM image of the fabricated multilayer stack (a) and line scan profile along vertical axis (b), indicating significant intermixing at the interface between CoFeB and W. Good fits to XRR measurements are only obtained if large W/CoFeB interface roughness $\lambda_{W/CoFeB}$ is assumed (c). The interface roughness does not change during annealing.

measurements of Fig. 5(c), which show that the W/CoFeB interface is very rough ($\lambda_{W/CoFeB} = 0.57$ nm), whereas a much smaller roughness is obtained for the CoFeB/MgO interface ($\lambda_{CoFeB/MgO} = 0.18$ nm). We note that $\lambda_{W/CoFeB}$ is not affected by thermal annealing of the sample, i.e., intermixing primarily occurs during film growth.

Strong intermixing between the W and CoFeB layers may explain large spin-orbit effect in W/CoFeB bilayers. It has been predicted theoretically that impurities may enhance the spin-orbit-coupling.[25] Indeed, in Ref. 26, the authors show that by adding heavy metal dopants into a ferromagnet, a significant increase of spin-orbit interaction can be observed. We therefore conclude that intermixing between W and CoFeB explains strong spin-orbit interactions in W/CoFeB bilayer leading to large planar and spin Hall effects as well as anisotropic and spin Hall magnetoresistance.[13]

In summary, we investigated spin-orbit torques in perpendicularly magnetized CoFeB on a thin W underlayer. Harmonic Hall voltage measurements were used to determine longitudinal and transverse spin-orbit effective magnetic fields. The damping-like spin-orbit torque component is found to increase with decreasing temperature reaching $\xi_L = 0.55$ at 19 K. The field-like torque magnitude also decreases with increasing temperature contrary to Ta buffers. Strong spin-orbit torques in W/CoFeB may be explained by a significant interface contribution. From TEM and XRR measurements, we conclude that the large interface effect originates from intermixing between the W and CoFeB layers.

We thank J. Barnaś and T. Taniguchi for a fruitful discussion and J. Chęciński for help in calculations. This work is partially supported by the National Science Center, Poland, Grant Harmonia No. UMO-2012/04/M/ST7/00799. W.S. acknowledges the National Science Center, Poland, Grant No. UMO-2015/17/D/ST3/00500. S.v.D. acknowledges financial support from the European Research Council (ERC-2012-StG 307502-E-CONTROL). L.Y. acknowledges financial support from the Academy of Finland (Grant Nos 286361 and 293929). Microfabrication was performed at Academic Center for Materials and Nanotechnology of AGH University. STEM analysis was conducted at the Aalto University Nanomicroscopy Center (Aalto-NMC).

[1]T. Kawahara, K. Ito, R. Takemura, and H. Ohno, Microelectron. Reliab. **52**, 613–627 (2012).
[2]R. L. Stamps, S. Breitkreutz, J. Akerman, A. V. Chumak, Y. Otani, G. E. W. Bauer, J.-U. Thiele, M. Bowen, S. A. Majetich, M. Kläui, I. L. Prejbeanu, B. Dieny, N. M. Dempsey, and B. Hillebrands, J. Phys. D: Appl. Phys. **47**, 333001 (2014).
[3]J. Sinova, D. Culcer, Q. Niu, N. A. Sinitsyn, T. Jungwirth, and A. H. MacDonald, Phys. Rev. Lett. **92**, 126603 (2004).
[4]I. M. Miron, G. Gaudin, S. Auffret, B. Rodmacq, A. Schuhl, S. Pizzini, J. Vogel, and P. Gambardella, Nat. Mater. **9**, 230–234 (2010).
[5]I. M. Miron, K. Garello, G. Gaudin, P.-J. Zermatten, M. V. Costache, S. Auffret, S. Bandiera, B. Rodmacq, A. Schuhl, and P. Gambardella, Nature **476**, 189–193 (2011).
[6]V. E. Demidov, S. Urazhdin, H. Ulrichs, V. Tiberkevich, A. Slavin, D. Baither, G. Schmitz, and S. O. Demokritov, Nat. Mater. **11**, 1028–1031 (2012).
[7]S. Emori, U. Bauer, S.-M. Ahn, E. Martinez, and G. S. D. Beach, Nat. Mater. **12**, 611–616 (2013).
[8]J. Kim, J. Sinha, M. Hayashi, M. Yamanouchi, S. Fukami, T. Suzuki, S. Mitani, and H. Ohno, Nat. Mater. **12**, 240–245 (2012).
[9]M. Akyol, J. G. Alzate, G. Yu, P. Upadhyaya, K. L. Wong, A. Ekicibil, P. Khalili Amiri, and K. L. Wang, Appl. Phys. Lett. **106**, 032406 (2015).
[10]L. Liu, T. Moriyama, D. C. Ralph, and R. A. Buhrman, Phys. Rev. Lett. **106**, 036601 (2011).
[11]Y. Niimi, M. Morota, D. H. Wei, C. Deranlot, M. Basletic, A. Hamzic, A. Fert, and Y. Otani, Phys. Rev. Lett. **106**, 126601 (2011).
[12]C.-F. Pai, M.-H. Nguyen, C. Belvin, L. H. Vilela-Leão, D. C. Ralph, and R. A. Buhrman, Appl. Phys. Lett. **104**, 082407 (2014).
[13]S. Cho, S.-h. C. Baek, K.-D. Lee, Y. Jo, and B.-G. Park, Sci. Rep. **5**, 14668 (2015).
[14]K.-U. Demasius, T. Phung, W. Zhang, B. P. Hughes, S.-H. Yang, A. Kellock, W. Han, A. Pushp, and S. S. P. Parkin, Nat. Commun. **7**, 10644 (2016).
[15]K. Garello, I. M. Miron, C. O. Avci, F. Freimuth, Y. Mokrousov, S. Blügel, S. Auffret, O. Boulle, G. Gaudin, and P. Gambardella, Nat. Nanotechnol. **8**, 587–593 (2013).
[16]W. Zhang, W. Han, X. Jiang, S.-H. Yang, and S. S. P. Parkin, Nat. Phys. **11**, 496–502 (2015).
[17]J.-C. Rojas-Sánchez, N. Reyren, P. Laczkowski, W. Savero, J.-P. Attané, C. Deranlot, M. Jamet, J.-M. George, L. Vila, and H. Jaffrès, Phys. Rev. Lett. **112**, 106602 (2014).
[18]J. Kim, J. Sinha, S. Mitani, M. Hayashi, S. Takahashi, S. Maekawa, M. Yamanouchi, and H. Ohno, Phys. Rev. B **89**, 174424 (2014).
[19]C.-F. Pai, L. Liu, Y. Li, H. W. Tseng, D. C. Ralph, and R. A. Buhrman, Appl. Phys. Lett. **101**, 122404 (2012).
[20]Q. Hao and G. Xiao, Phys. Rev. Appl. **3**, 034009 (2015).
[21]W. Skowroński, T. Nozaki, D. D. Lam, Y. Shiota, K. Yakushiji, H. Kubota, A. Fukushima, S. Yuasa, and Y. Suzuki, Phys. Rev. B **91**, 184410 (2015).
[22]J. Torrejon, J. Kim, J. Sinha, S. Mitani, M. Hayashi, M. Yamanouchi, and H. Ohno, Nat. Commun. **5**, 4655 (2014).
[23]J.-V. Kim, Solid State Phys. **63**, 217–294 (2012).
[24]S. Cho and B.-G. Park, Curr. Appl. Phys. **15**, 902–905 (2015).
[25]T. P. Pareek and P. Bruno, Pramana **58**, 293–311 (2002).
[26]A. Hrabec, F. J. T. Goncalves, C. S. Spencer, E. Arenholz, A. T. N'Diaye, R. L. Stamps, and C. H. Marrows, Phys. Rev. B **93**, 014432 (2016).